# A study of practical implementations of the Overlap-Dirac operator in four dimensions

Robert G. Edwards, Urs M. Heller and Rajamani Narayanan

*SCRI, The Florida State University, Tallahassee, FL 32306-4130, USA*

**Abstract**

We study three practical implementations of the Overlap-Dirac operator $\not{D}_o = \frac{1}{2}[1 + \gamma_5 \epsilon(\mathrm{H}_w)]$ in four dimensions. Two implementations are based on different representations of $\epsilon(\mathrm{H}_w)$ as a sum over poles. One of them is a polar decomposition and the other is an optimal fit to a ratio of polynomials. The third one is obtained by representing $\epsilon(\mathrm{H}_w)$ using Gegenbauer polynomials and is referred to as the fractional inverse method. After presenting some spectral properties of the Hermitian operator $\mathrm{H}_o = \gamma_5 \not{D}_o$, we study its spectrum in a smooth SU(2) instanton background with the aim of comparing the three implementations of $\not{D}_o$. We also present some results in SU(2) gauge field backgrounds generated at $\beta = 2.5$ on an $8^4$ lattice. Chiral properties have been numerically verified.

**PACS #:** 11.15.Ha, 11.30.Rd, 11.30.Fs
Key Words: Lattice QCD, Algorithms, Chiral fermions, Topology.

## 1 Introduction

The overlap formalism provides a way of realizing exact chiral symmetry on the lattice. For vector gauge theories, there is now promise that this formalism can be made practical. The Overlap-Dirac operator derived from the overlap formalism [1] of chiral fermions is [2]

$$\not{D}_o = \frac{1}{2}[1 + \gamma_5 \epsilon(\mathrm{H}_w)]; \qquad \epsilon(\mathrm{H}_w) = \frac{\mathrm{H}_w}{|\mathrm{H}_w|} \tag{1}$$

where

$$H_w = \begin{pmatrix} B - m & C \\ C^\dagger & -B + m \end{pmatrix} ; \tag{2}$$

$$C_{i\alpha,j\beta}(n, n') = \frac{1}{2} \sum_\mu \sigma_\mu^{\alpha\beta} [U_\mu^{ij}(n)\delta_{n',n+\hat{\mu}} - (U_\mu^\dagger)^{ij}(n')\delta_{n,n'+\hat{\mu}}] \tag{3}$$

$$B_{i\alpha,j\beta}(n, n') = \frac{1}{2}\delta_{\alpha,\beta} \sum_\mu [2\delta_{ij}\delta_{nn'} - U_\mu^{ij}(n)\delta_{n',n+\hat{\mu}} - (U_\mu^\dagger)^{ij}(n')\delta_{n,n'+\hat{\mu}}] \tag{4}$$

is the Hermitian Wilson-Dirac operator. We will refer to $m$ as the overlap mass. This is a parameter that has to be in the range $(0, 2)$ for $\not{D}_o$ to describe a single massless Dirac fermion. In principle, any value of $m$ in this region will yield the same continuum theory. But at finite lattice spacing the cutoff effects can be quite different, for different choices of $m$. In particular one needs $m > m_1(g^2)$, for some $m_1(g^2)$ going to zero in the continuum limit, in order for the overlap fermions to "feel the topology of background gauge fields"[4].

It is necessary to efficiently deal with the action of $\epsilon(H_w)$ on a vector for practical implementations of this operator in four dimensional theories. Recently, one representation of $\epsilon(x)$ as a sum of poles of $x^2$ was used to demonstrate that a practical implementation of the Overlap-Dirac operator is possible in three dimensions [5]. One can also represent $\epsilon(x)$ as an optimal rational function [6]. Another approach is to use Gegenbauer polynomials to represent $\frac{1}{\sqrt{x^2}}$ resulting in an iterative procedure to compute the action of $\epsilon(H_w)$ on a vector [7]. In this paper we compare these three methods from a practical point of view. We start by presenting some spectral properties of $H_o = \gamma_5 \not{D}_o$ and $\not{D}_o$ and then use a smooth SU(2) instanton background as an example to illustrate these spectral properties. The example will also enable us to compare the three practical implementations of $\epsilon(H_w)$. We also present some results in SU(2) gauge field backgrounds at $\beta = 2.5$ on an $8^4$ lattice.

## 2  Spectral properties of $\not{D}_o$

In this section, we build on some results of Neuberger [2,3] by considering the eigenvalue problem of the Hermitian Overlap-Dirac operator,

$$H_o = \gamma_5 \not{D}_o = \frac{1}{2}[\gamma_5 + \epsilon(H_w)] \quad . \tag{5}$$

We do not use the explicit expression for $H_w$ in this section and we only use the fact that $\epsilon^2(H_w) = 1$. The exact chiral symmetry built into the overlap formalism has been reemphasized in the context of the fermionic action with $\not{D}_o$ in Ref. [8]. We therefore expect the spectrum of $H_o$ to essentially reproduce all the important continuum properties. The spectral properties of the continuum operator $H = \gamma_5 \not{D}$ are

- Exact zero eigenvalues of H are associated with topology. The associated eigenvectors are also eigenvectors of $\gamma_5$. The zero eigenvalues are not paired in any sense. We can have $n_+$ zero eigenvalues with positive chirality and $n_-$ zero eigenvalues with negative chirality. The difference $(n_+ - n_-)$ is the topology of the background gauge field.
- Non-zero eigenvalues of H come in pairs that are equal in magnitude and opposite in sign. The associated eigenvectors are not eigenvectors of $\gamma_5$, but rather $\gamma_5$ has zero expectation value in the eigenvectors, $\psi^\dagger \gamma_5 \psi = 0$.

On a finite four dimensional lattice, the matrix $H_o$ is a finite even dimensional matrix and $\det H_o$ is the overlap formula in a fixed gauge background. The overlap exactly vanishes if the topology is non-trivial; therefore, $H_o$ should have exact zero modes in a gauge field background that is topologically non-trivial. These zero modes should have definite chirality and the difference in the positive and negative modes is the topology of the gauge field. If the topology is odd, then $H_o$ should have an odd number of exact zero modes. Therefore it should also have an odd number of non-zero modes. This implies that the number of positive eigenvalues cannot be equal to the number of negative eigenvalues. It is then interesting to explore the properties of the spectrum of $H_o$ with the aim of establishing the equivalence of the two continuum properties listed above. We prove the following properties of $H_o$ on the lattice:

- The spectrum of $H_o$ is bounded by the region $[-1, 1]$.
- Zero eigenvalues of $H_o$ have a definite chirality and need not occur in pairs. Eigenvalues of $H_o$ equal to $\pm 1$ also have definite chirality. These eigenvalues also need not occur in pairs.
- Non-zero eigenvalues of $H_o$ that have a magnitude less than one come in pairs that are equal in magnitude and opposite in sign, namely $\pm\lambda$. The associated eigenvectors are not eigenvectors of $\gamma_5$, but rather $\gamma_5$ has expectation value $\pm\lambda$ in the eigenvectors, $\psi^\dagger \gamma_5 \psi = \pm\lambda$ for $H_o \psi = \pm\lambda \psi$.

Since $H_o$ is an even dimensional matrix, the unpaired zero eigenvalues have to be matched by unpaired eigenvalues equal to $\pm 1$. This is what is expected to happen in a topologically non-trivial background.

We present the proofs to the properties of $H_o$ listed above.

- Squaring $H_o$ in (5) we get

$$H_o^2 = \frac{1}{4}\Big[2 + \gamma_5 \epsilon(H_w) + \epsilon(H_w)\gamma_5\Big] \tag{6}$$

The above equation can be rewritten using (5) as

$$2H_o^2 = \gamma_5 H_o + H_o \gamma_5 \tag{7}$$

3

and is commonly referred to as the Ginsparg-Wilson relation. As pointed out in [2], $\gamma_5 \epsilon(H_w)$ is an unitary operator and $\epsilon(H_w)\gamma_5$ is its Hermitian conjugate. Therefore, all the eigenvalues of $[\gamma_5\epsilon(H_w)+\epsilon(H_w)\gamma_5]$ are bounded by $[-2,2]$. Therefore all eigenvalues of $H_o^2$ are bounded by $[0,1]$ and from this the first property of $H_o$ follows.

- Let us first find all eigenvectors of $H_o$ that are also eigenvectors of $\gamma_5$. Let $\psi$ be an eigenvector of $H_o$ with eigenvalue $\lambda$ and let $\gamma_5\psi = \pm\psi$. With the aid of (7) one concludes that $\lambda(\lambda \mp 1) = 0$. Therefore we have either $\lambda = 0$ or $\lambda = \pm 1$, and we have shown that chiral eigenvectors of $H_o$ have eigenvalues equal to zero or $\pm 1$. The subspace spanned by the zero eigenvalues of $H_o$ can be split into two further subspaces. One with dimension of $n_+$ will have positive chirality and one with dimension of $n_-$ will have negative chirality. The number $n_+$ need not be equal to $n_-$ and if $(n_+ - n_-)$ is not equal to zero then the gauge field carries a non-trivial topology. All eigenvalues of $H_o$ equal to $+1$ have positive chirality and vice-versa.

- Let $0 < \lambda < 1$ be an eigenvalue of $H_o$ with eigenvector $\psi$ that is normalized to unity. Clearly,

$$\phi = \frac{\gamma_5\psi - (\psi^\dagger\gamma_5\psi)\psi}{\sqrt{1 - (\psi^\dagger\gamma_5\psi)^2}}; \qquad \psi^\dagger\phi = 0 \tag{8}$$

is a new vector that is orthonormal to $\psi$ since $\psi^\dagger\gamma_5\psi \neq \pm 1$. We can now compute $H_o\phi$ using the Ginsparg-Wilson relation, (7), and find that

$$H_o\phi = -\lambda\phi + \frac{2\lambda(\lambda - \psi^\dagger\gamma_5\psi)}{\sqrt{1 - (\psi^\dagger\gamma_5\psi)^2}} \cdot \psi \tag{9}$$

This shows that $H_o$ acting on the subspace spanned by $(\psi, \phi)$ results in vectors in that subspace. From $H_o\psi = \lambda\psi$ and $\phi^\dagger\psi = 0$, it follows that $\phi^\dagger H_o\psi = 0$. From the hermiticity of $H_o$, we also have $\psi^\dagger H_o\phi = 0$. This along with (9) results in

$$\psi^\dagger\gamma_5\psi = \lambda \tag{10}$$

since we have assumed $\lambda \neq 0$. We have also assumed that $\lambda \neq 1$ in the beginning and therefore $\phi$ is indeed a non-zero vector with

$$H_o\phi = -\lambda\phi; \quad \phi = \frac{\gamma_5\psi - \lambda\psi}{\sqrt{1 - \lambda^2}} \quad . \tag{11}$$

This establishes the last property of $H_o$.

Comparing the properties of $H_o$ with the desired properties of $H$ in the continuum, we conclude that $H_o$ reproduces topology correctly, as expected. The eigenvectors of the non-zero eigenvalues of $H_o$ do not have a zero expectation value of $\gamma_5$. Eigenvalues of $H_o$ have to be scaled by the lattice spacing to get

the eigenvalues of the continuum operator and then only the eigenvalues of $H_o$ close to zero have a continuum relevance. The last property tells us that the corresponding eigenvectors also have an expectation value of $\gamma_5$ close to zero as expected in the continuum.

It is trivial to find the eigenvalues and left eigenvectors of $\slashed{D}_o$ since $\slashed{D}_o$ also maps the subspace spanned by $(\psi, \phi)$ onto itself. The eigenvalues of $\slashed{D}_o$ are zero when $\lambda = 0$, unity when $\lambda = \pm 1$ and the complex conjugate pairs $(\lambda^2 \pm i\lambda\sqrt{1-\lambda^2})$ for $0 < \lambda < 1$. This proves that the only real eigenvalues of the Overlap-Dirac operator are zero and unity. The massive Overlap-Dirac operator is given by $\slashed{D}_o + m_f$ with $-1/2 < m_f < \infty$ [9] [1] . Clearly the operator has a zero eigenvalue only when $m_f = 0$. Occurrence of zero eigenvalues for a lattice Dirac operator at positive quark masses in certain gauge field backgrounds are referred to as "exceptional" configurations. Such "exceptional" configurations are actually generic for the Wilson-Dirac operator but non-existent for the Overlap-Dirac operator. As pointed out in Ref. [10] the only difficulty arises in defining the Overlap-Dirac operator if $H_w$ has a zero eigenvalue since $\epsilon(H_w)$ is then not well defined. In such a background configuration, one can define the operator at a value of $m$ slightly away from the one where $H_w$ has a zero eigenvalue since the continuum limit is expected to be independent of $m$.

Finally, one can also trivially get the spectral flow of the massive $H_o(m_f)$. If $H_o(0)$ has a zero eigenvalue then $H_o(m_f)$ has an eigenvalue equal to $\pm m_f$ corresponding to positive and negative chirality of the eigenvector. If $H_o(0)$ has an eigenvalue equal to $\pm 1$, then $H_o(m_f)$ has an eigenvalue equal to $\pm(1+m_f)$. For the paired eigenvalues $\pm\lambda$ of $H_o(0)$ in the range $0 < \lambda < 1$, $H_o(m_f)$ has paired eigenvalues equal to $\pm\sqrt{\lambda^2 + 2\lambda^2 m_f + m_f^2}$. This again shows that zero crossings in the region $-1/2 < m_f < \infty$ occur only at $m_f = 0$ and these are due to the topological content of the gauge field.

## 3  Algorithms

The key element in the application of the Overlap-Dirac operator (1) on a vector is how to apply $\epsilon(H_w)$ on a vector. The meaning of $\epsilon(H_w)$ is defined through the $\epsilon$ function on the eigenvalues of $H_w$. Hence, the diagonalization of $H_w$ is one possible method and has been applied in two dimensional systems [11]. However, on larger systems of interest, exact diagonalization is prohibitive.

---

[1]   The fermion mass $m_f$ should be written as $m_f = \frac{\mu}{1-\mu}$ with $\mu$ in the range $[-1, 1]$. Positive values of $\mu$ correspond to positive quark masses and vice-versa. [9]

## 3.1 Fractional inverse method

By representing $\epsilon(\mathrm{H}_w)$ as

$$\epsilon(\mathrm{H}_w) = \left(\mathrm{H}_w^2\right)^{-1/2} H_w \tag{12}$$

we can directly apply $\epsilon(\mathrm{H}_w)$ on a vector by using a Krylov space iterative solver for the fractional inverse based on Gegenbauer polynomials [7]. In this method, one parameterizes the system to be solved,

$$M^\gamma \phi = \chi \quad , \tag{13}$$

by

$$M = c(1 + t^2 - 2tA) \quad , \tag{14}$$

The key to solving (13) is then the generating function for Gegenbauer polynomials

$$(1 + t^2 - 2tA)^{-\gamma} = \sum_{n=0}^{\infty} t^n C_n^\gamma(A) \quad . \tag{15}$$

Using the recursion relations for the $C_n^\gamma$ one can construct an iterative solver for $\phi$ in (13). We refer the reader to [7] for details. For the case of interest, $\gamma = 1/2$ and $M = \mathrm{H}_w^2$ is hermitian and positive (semi-)definite. We restrict the bounds of $A$ to be in $[-1, 1]$ and obtain uniform convergence of $A$ and hence $M = \mathrm{H}_w^2$ in (15) provided $|t| < 1$. It is important for the best convergence to match the extremal eigenvalues of $\mathrm{H}_w^2 \in [\lambda_{min}^2, \lambda_{max}^2]$ to those of $A \in [-1, 1]$. Then, the $t$ and $c$ are determined and

$$t = 1 - \frac{1}{\kappa}, \tag{16}$$

where $\kappa = |\lambda_{max}/\lambda_{min}|$ is the condition number of $\mathrm{H}_w$. The parameter $t$ is the convergence factor for the algorithm. Typically, $\lambda_{max} \lesssim 8$, but $|\lambda_{min}|$ can be quite small [4]. Control of the lowest mode is important since the number of iterations expected to reach a given accuracy $R$ is bounded by $-\log(R)\kappa$, and numerical tests have shown this bound to be saturated. We remark that the same bound also applies to the Conjugate Gradient (CG) algorithm but is not expected to be saturated. The polynomials generated by the Gegenbauer expansion are not optimal, while the CG algorithm is optimal. Eigenvectors with small eigenvalue can be projected out of (12) to improve convergence.

## 3.2  Pole methods

### 3.2.1  Polar decomposition

Another approach is to consider $\epsilon(z)$ as the limit of some function that switches quickly between $\pm 1$ on $z$ changing sign. Recently, Neuberger showed [5,12] that

$$\epsilon(z) = \lim_{N \to \infty} f_N(z), \tag{17}$$

with

$$f_N(z) = \frac{(1+z)^{2N} - (1-z)^{2N}}{(1+z)^{2N} + (1-z)^{2N}} \quad . \tag{18}$$

In particular, $f_N(z)$ provides a good approximation for $\epsilon(z)$ at finite $N$ for $1/N \lesssim z \lesssim N$, and can be expressed quite simply, by matching poles and residues, as a sum over poles

$$f_N(z) = z \sum_{k=1}^{N} \frac{a_k}{z^2 + b_k} \tag{19}$$

$$a_k = \frac{1}{N \cos^2(\frac{\pi}{2N}(k - \frac{1}{2}))} \ , \qquad b_k = \tan^2(\frac{\pi}{2N}(k - \frac{1}{2})) \quad . \tag{20}$$

Since $\epsilon(sz) = \epsilon(z)$ for positive $s$, the argument $z$ can be rescaled into the region suitable for the approximation. For the application of $f_N(\mathrm{H}_w)$ on a vector, one can use a multi–shift CG solver [13] for the $N$ terms in $f_N(\mathrm{H}_w)$ [5]. The convergence is governed by the smallest shift; however, the overall cost is not much more than the inversion for the smallest shift. The representation of $f_N(\mathrm{H}_w)$ in terms of poles is the key observation to making the algorithm practical.

While the smallest shift, $b_1$, in (20) governs convergence, the choice of $N$ is determined by the condition number of $\mathrm{H}_w$. The optimal choice for the scale factor $s$ is $\frac{1}{\sqrt{\lambda_{max}\lambda_{min}}}$. The maximum deviation of $f_N(sz)$ away from unity occurs at $z = \lambda_{max}$ and $z = \lambda_{min}$, and the maximum deviation monotonically decreases in $N$. The desired accuracy $\delta$ over the spectral range of $\mathrm{H}_w$ fixes $N$ depending on the condition number $\kappa$, namely $N = 0.25\sqrt{\kappa}\ln\frac{\delta}{2}$. Hence, the condition number is the real measure of convergence for small $\lambda_{min}$ if a good uniform approximation is to be achieved. This requirement may not be needed in practice as long as the lowest modes are well represented, but will be used throughout this work since it is not difficult to achieve.

### 3.2.2 Optimal rational approximation

Other approximations to $\epsilon(z)$ over a finite interval can be suggested. A polynomial approximation like Chebyshev over the interval $[-1, 1]$ is particularly bad since it is only logarithmically convergent. A better choice is the ratio of polynomials called an optimal rational function approximation. Since $\epsilon(z)$ is odd, we choose the form

$$g_N(z) = z\frac{P_N(z^2)}{Q_N(z^2)} \qquad (21)$$

where we assume the polynomials are irreducible of degree $N$. We choose the highest order coefficient in $Q_N(z)$ to be one. The normalization is contained in $P_N(z)$ and is defined to be $c_0$. As in the previous section, since $\epsilon(sz) = \epsilon(z)$ for positive $s$, the argument $z$ can be rescaled into the region suitable for the approximation.

To cast into a suitable form, we change variables to $y = z^2$ and consider $h(y) = (1/z)\epsilon(z)$ over the interval $[0, z_{max}^2]$. One can show [14] that there exist best approximations of $r(y) = P_N(y)/Q_N(y)$ for a continuous function in a uniform norm over the interval $[y_{min}, 1]$ (with no loss of generality, we restrict the upper bound). The deviation of $r(y)$ from the intended function $1/\sqrt{y}$ can be shown [14] to have $2 + 2N$ extrema with two always the endpoints. An algorithm, sometimes called the Remez algorithm [6,14,15], exists to find the best approximation $r(y)$. The version used here requires the extrema of the relative error to be constant. For our application, this implies the worst error in $g_N(z)$ is for the smallest $z$. Other weighting functions can be chosen.

The numerical evaluation of (21) is most stable in factored form

$$g_N(z) = zc_0\frac{\prod_{k=1}^{N}(z^2 + p_k)}{\prod_{k=1}^{N}(z^2 + q_k)} \qquad (22)$$

where we find the roots $p_k$ and $q_k$ to be real and positive. We can cast this expression as a sum over poles as in Section 3.2.1:

$$g_N(z) = z\left(c_0 + \sum_{k=1}^{N}\frac{c_k}{z^2 + q_k}\right); \qquad c_k = c_0\frac{\prod_{i=1}^{N}(q_k - p_i)}{\prod_{i=1,i\neq k}^{N}(q_k - q_i)} \qquad (23)$$

We choose the value of $N$ so that the deviations of $|g_N(z)|$ over the interval $[z_{min}, 1]$ are some acceptably small value $\delta$. We show examples in Fig. 3 of $N = 6, 8$ and $10$ for the fit interval $[0.005, 1]$, which admits a condition number of 200. We see the method rapidly converges in $N$. In our tests, we have chosen $N = 8$ where we see less than 0.5% of an error. However, we observe that since

we are approximating a flat function, we can in practice extend the acceptable upper bound beyond 1. For $z > 1$, $g_N(z)$ monotonically increases. For $N = 8$, we can choose $z_{max} = 2.8$ and still maintain a 1% error. We can use this trick to effectively increase the useful allowable condition number to over 500. In Table 1, we show the roots and normalizations for the polynomials shown in Fig. 3.

## 4  Results

We will consider a gauge field background with a single SU(2) instanton to compare the performance of the three algorithms described in the previous section. The SU(2) link elements on the lattice obtained from an exact evaluation of the path ordered integral of the continuum instanton take the following form [16]. In the singular gauge,

$$U_\mu(n) = \exp\left[ib_\mu(n) \cdot \sigma(\vartheta_\mu(n;0) - \vartheta_\mu(n;\rho))\right] \tag{24}$$

$$\vartheta_\mu(n;\rho) = \frac{1}{\sqrt{\rho^2 + \sum_{\nu\neq\mu}(n_\nu - c_\nu)^2}} \tan^{-1} \frac{\sqrt{\rho^2 + \sum_{\nu\neq\mu}(n_\nu - c_\nu)^2}}{\rho^2 + \sum_\nu(n_\nu - c_\nu)^2 + (n_\mu - c_\mu)} \tag{25}$$

$$
\begin{aligned}
b_1(n) &= (-n_4 + c_4, n_3 - c_3, -n_2 + c_2), \\
b_2(n) &= (-n_3 + c_3, -n_4 + c_4, n_1 - c_1), \\
b_3(n) &= (n_2 - c_2, -n_1 + c_1, -n_4 + c_4), \\
b_4(n) &= (n_1 - c_1, n_2 - c_2, n_3 - c_3)
\end{aligned}
\tag{26}
$$

Here $c$ denotes the center of the instanton, and $\rho$ is the size of the instanton measured in lattice units. We work on an $8^4$ periodic lattice and set $\rho = 1.5$ and $c_\mu = 4.5$ with the lattice sites in each direction numbered from 1 to 8.

We first present the results. We used the explicitly real representation of $H_w$ [3]. We computed a few low lying eigenvalues of $H_o$ using the Ritz algorithm [17] to compute the lowest eigenvalues of $H_o^2$. From our previous work on the spectral flow of the hermitian Wilson-Dirac operator, we know that a level of $H_w$ crosses zero between $m = 0.5$ and $m = 0.6$ [18]. This flow is shown as a solid line in Fig. 1. The low lying eigenvalues of $H_o$ as a function of $m$ are also shown in the same figure as octagons. For $0 \leq m \leq 0.5$, fourteen low lying eigenvalues are shown and for $0.6 \leq m \leq 0.9$ fifteen low lying eigenvalues are shown. The non-zero eigenvalues come in opposite pairs with their chirality being equal to their eigenvalue. This is in accordance with the last property of $H_o$. The seven positive and the seven negative eigenvalues are nearly degenerate. For $0.6 \leq m \leq 0.9$, there is a single zero eigenvalue for $H_o$. This is due

9

to the instanton background. The abrupt appearance of a zero eigenvalue with chirality $+1$ is accompanied with the appearance of an eigenvalue of $-1$ with chirality $-1$. It is difficult to confirm this numerically because of the observed high density of eigenvalues near $\pm 1$. The shape of the zero mode for $0.6 \leq m \leq 0.9$ is shown in Fig. 2. The $z(t)$ plotted is equal to $\sum_{\vec{x}a} \psi^2(\vec{x}, t, a)$ and the continuum mode is plotted as a solid line. The zero mode is remarkably stable under change of the overlap mass $m$.

We have made comparisons of the average number of $H_w^2$ operations to obtain the result of the action of $\epsilon(H_w)$ on a vector. The average is over all the Ritz iterations needed in solving for the lowest eigenvalue in Fig. 1. The main comparison is between the pole method and the fractional inverse method. The two pole methods are expected to be comparable in the average number of $H_w^2$ operations on a vector. Since we are using the method of pole shifts the number of poles only affect the memory requirement and some additional multiplications of vectors by scalars and additions of vectors. We show in Fig. 4 the scaling of the number of $H_w^2$ operations versus the condition number $\kappa$ of $H_w$ at masses below and above the crossing. We used the $N = 8$ polynomial in Tab. 1 (c.f. Eq. (23)). The fractional inverse method scales quite linearly in $\kappa$ and the $H_w^2$ operation count grows to large values while in the optimal rational approximation it grows very slowly. This is because the bound on the rate of convergence is saturated in the fractional inverse method while in CG it is not. As expected, no substantial difference in the number of $H_w^2$ operations was found between a $N = 50$ order $f_N(H_w)$ in Eq. (20) and the $N = 8$ optimal rational approximation.

Although the two pole methods need similar number of $H_w^2$ operations there are some differences. For a fixed accuracy (maximum deviation $\delta$ away from unity in the realization of $\epsilon(z)$) and a fixed condition number the number of poles needed in the optimal rational approximation is smaller than the one needed in the polar decomposition. For example, with $\delta = 0.01$, the optimal rational approximation needs seven poles for a condition number of 200 and twelve poles for a condition number of 1000. In contrast, the polar decomposition needs 19 poles for a condition number of 200 and 42 poles for a condition number of 1000. This indicates that the number of poles needed grows with the condition number at a slower rate in the optimal rational approximation than in the polar decomposition.

A comparison of the number of poles needed for the optimal rational approximation as a function of the accuracy for a fixed condition number is shown in Fig. 5. The number of poles needed depends logarithmically on the accuracy, $\delta$, and the slope is smaller for larger condition number. As mentioned before, the number of poles needed only affects the memory requirement and results in a few additional operations of two types: addition of two vectors and multiplication of vector by a scalar. For a fixed memory requirement, the optimal

rational approximation will admit a larger condition number.

We also present the results of the spectral flow of $H_o$ in three pure SU(2) gauge field backgrounds generated at $\beta = 2.5$ on an $8^4$ lattice to further emphasize the feasibility of the algorithms described here. The flows are shown in Fig. 6–8. Fig. 6 is the flow in a background that contains a single instanton and this results in an exact zero mode of $H_o$. We verified that it is an exact zero mode by computing its chirality which was found to be equal to $-1$. Fig. 7 is the flow in a background that has no topological object and we do not find any exact zero mode in this case. Fig. 8 is the flow in a background that contains an instanton and an anti-instanton. These will result in approximate zero modes and one can see evidence for this in the sharp drop in the flow between $m = 0.6$ and $m = 0.7$ and also by comparing to the flow in Fig. 7. The modes in Fig. 8 are definitely not exact zero modes and, in accordance with the last property of $H_o$, have chiralities equal to their eigenvalues. Finally we also show the exact zero mode found in the flow in Fig. 6. We plot it for all $m > 0.8$ and find that the mode is essentially the same and it also agrees with the zero mode of $H_w$ computed close to the point in $m$ where $H_w$ has a zero crossing.

## 5   Concluding remarks

We have compared three implementations of the Overlap-Dirac operator in four dimensions. We find that the pole methods are superior in convergence to the fractional inverse method. The main advantage of the optimal rational function approximation is that a suitable error can be achieved for a smaller order polynomial. This saves some work in the multi-shift CG since fewer vectors are need. Also, memory can be saved. No difference in convergence properties is expected otherwise.

For the massive Overlap-Dirac operator, one can again use the multi-shift CG solver [13] to solve for the inverse with several quark masses. The action of $\epsilon(H_w)$ is only applied on one vector and the quark masses can be expressed as a shift.

In practice it may be worth projecting out a few small eigenvectors of $H_w$ before the action of $\epsilon(H_w)$ on a vector. This is useful if there are a few well separated small eigenvalues. The projection can have a dramatic effect in the fractional inverse method since the number of $H_w^2$ operations is linear in the condition number. It will also decrease the operation count in the pole methods. We have verified these effects on the configurations studied in this paper.

The pairing of the non-zero eigenvalues of $H_o$ can be used to reduce the com-

putation of the spectrum of $H_o$.

We have demonstrated the feasibility of using the Overlap-Dirac operator in a four dimensional gauge theory by computing the spectral flow of $H_o$ in SU(2) gauge field backgrounds at $\beta = 2.5$ on an $8^4$ lattice. Chiral properties have been shown to be properly reproduced. Exact zero modes have been shown to be related to topology. They are clearly differentiated from almost zero modes in that the exact zero modes have chirality $\pm 1$ while the almost zero modes have chirality equal to their eigenvalue, namely very small.

## Acknowledgements

## References

[1] R. Narayanan and H. Neuberger, *Nucl. Phys.* **B443** (1995) 305.

[2] H. Neuberger, *Phys. Lett.* **B417** (1998) 141.

[3] H. Neuberger, hep-lat/9803011.

[4] R.G. Edwards, U.M. Heller and R. Narayanan, hep-lat/9802016.

[5] H. Neuberger, hep-lat/9806025.

[6] E. Ya. Remez, *General Computational Methods of Chebyshev Approximations. The Problems of Linear Real Parameters*, AEC-tr-4491, U.S. Atomic Energy Commission, 1962; H.J. Maehly, *Methods for Fitting Rational Approximations, Parts II and III*, Association for Computing Machinery Journal, 10, 257–277 (1963).

[7] B. Bunk *Nucl. Phys. Proc. Suppl.* **B63** (1998) 952.

[8] M. Lüscher, hep-lat/9802011.

[9] H. Neuberger, *Phys. Rev.* **D57** (1998) 5417.

[10] H. Neuberger, hep-lat/9801031.

[11] Y. Kikukawa, R. Narayanan and H. Neuberger, *Phys. Rev.* **D57** (1998) 1233; R. Narayanan, H. Neuberger and P. Vranas, *Phys. Lett.* **B353** (1995) 507.

[12] N.J. Higham, Linear Algebra and Appl., Proceedings of ILAS Conference "Pure and Applied Linear Algebra: The New Generation", Pensacola, March 1993.

[13] A. Frommer, S. Güsken, T. Lippert, B. Nöckel, K. Schilling, Int. J. Mod. Phys. **C6** (1995) 627; B. Jegerlehner, hep-lat/9612014.

[14] *An Introduction to the Approximation of Functions*, T. Rivlin, Dover Publications, 1981.

[15] S.L.Moshier, *Methods and Programs for Mathematical Functions*, Halsted Press, New York, 1989. Code available from http://www.netlib.org/cephes/remes.shar.

[16] M.L. Laursen, J. Smit and J.C. Vink, *Nucl. Phys.* **B343** (1990) 522.

[17] B. Bunk, K. Jansen, M. Lüscher and H. Simma, DESY-Report (September 1994); T. Kalkreuter and H. Simma,*Comput. Phys. Commun.* **93** (1996) 33.

[18] R.G. Edwards, U.M. Heller and R. Narayanan, *Nucl. Phys.* **B522** (1998) 285.

| $c_0^{(6)} = 0.182031$ | | $c_0^{(8)} = 0.138827$ | | $c_0^{(10)} = 0.112209$ | |
| --- | --- | --- | --- | --- | --- |
| $P_6$ | $Q_6$ | $P_8$ | $Q_8$ | $P_{10}$ | $Q_{10}$ |
| 2.05911386e-04 | 2.59134855e-05 | 8.76771341e-05 | 1.41842155e-05 | 4.66940445e-05 | 8.66147628e-06 |
| 4.41581797e-03 | 1.09739974e-03 | 1.23623252e-03 | 3.61450316e-04 | 4.91389639e-04 | 1.63943675e-04 |
| 3.77980526e-02 | 1.40770643e-02 | 9.11319209e-03 | 3.60062816e-03 | 3.13861891e-03 | 1.31054157e-03 |
| 2.01546314e-01 | 9.03340757e-02 | 4.26239090e-02 | 2.05879480e-02 | 1.36974237e-02 | 6.82851948e-03 |
| 1.00302812e+00 | 4.40335697e-01 | 1.54018532e-01 | 8.27820958e-02 | 4.57939021e-02 | 2.57134015e-02 |
| 1.18344772e+01 | 2.67694284e+00 | 5.10199622e-01 | 2.80210832e-01 | 1.30067127e-01 | 7.83188602e-02 |
| | | 1.96142588e+00 | 9.59252529e-01 | 3.43184790e-01 | 2.12031104e-01 |
| | | 2.06291295e+01 | 4.86700520e+00 | 9.33072953e-01 | 5.59010141e-01 |
| | | | | 3.19171360e+00 | 1.64058378e+00 |
| | | | | 3.17877409e+01 | 7.65233478e+00 |

Table 1

The normalization and roots for the optimal rational function approximation to $\epsilon(z)$ (Eq. 22) over the interval $[0.005, 1]$ for $N = 6, 8$ and 10.
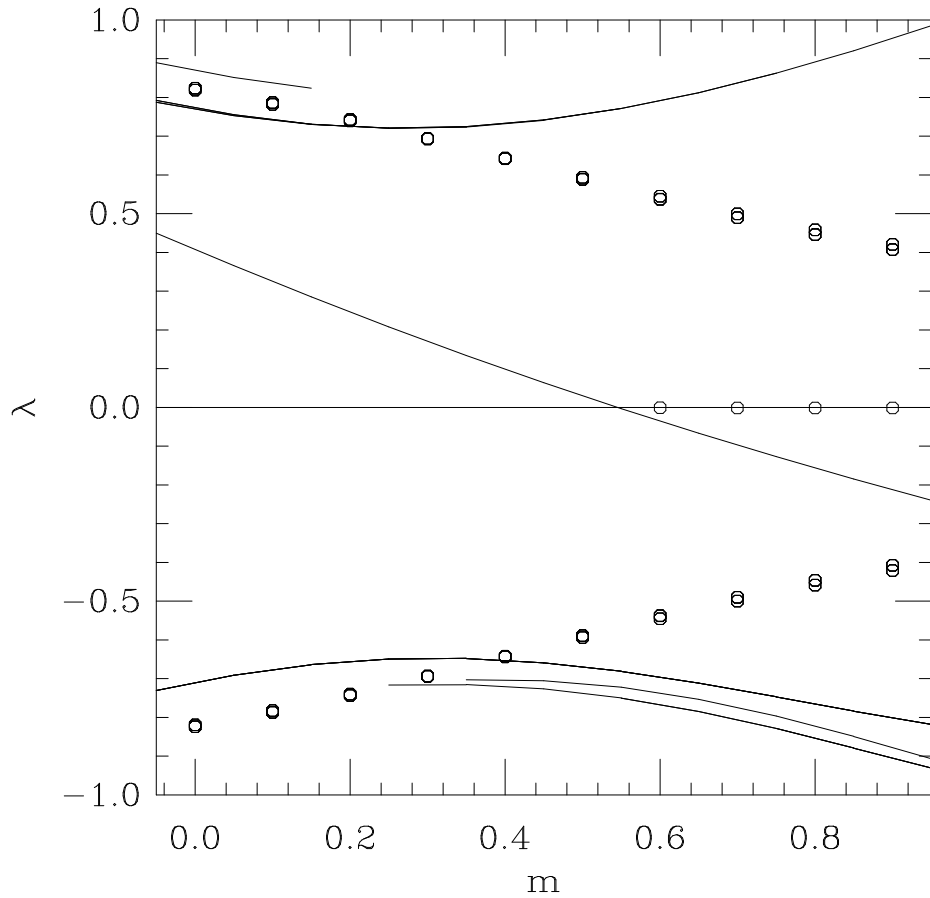
Fig. 1. The octagons describe the low lying spectrum of $H_o$ in an smooth SU(2) instanton background. The zero mode found at $m > 0.5$ is singly degenerate and is associated with the instanton. The lines are the spectral flow of $H_w$.
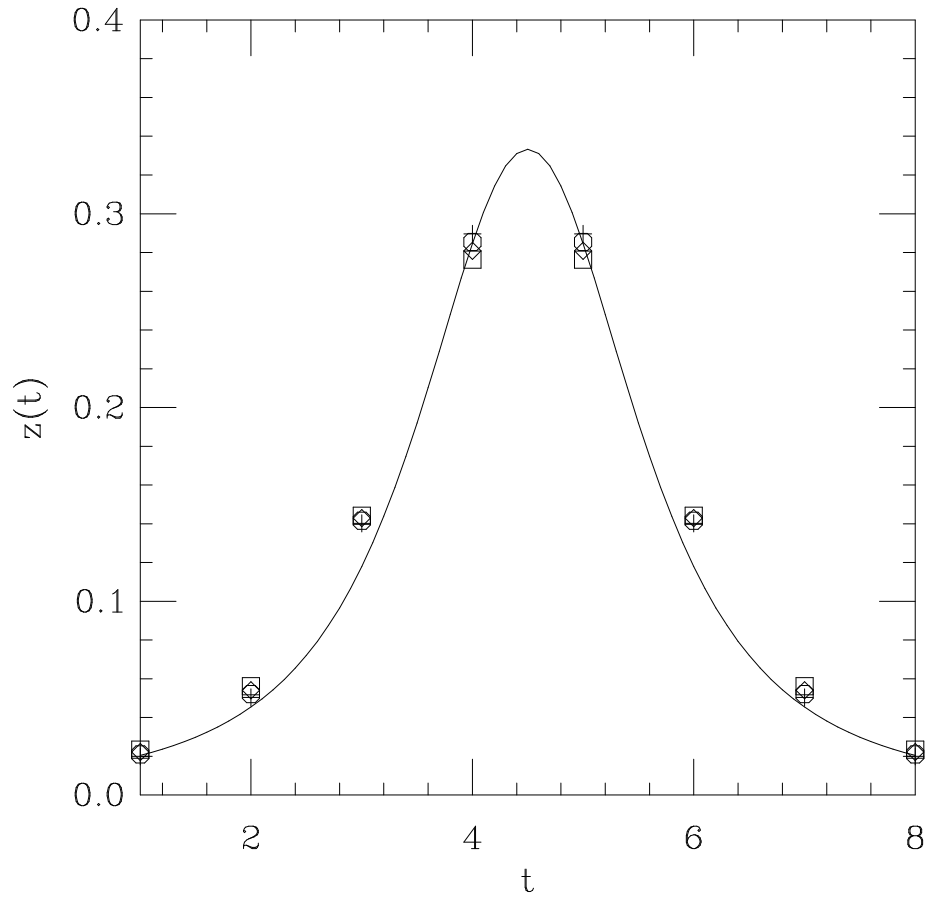
Fig. 2. The mode associated with the zero eigenvalues in Fig. 1 at $m = 0.6$ (square), $m = 0.7$ (diamond). $m = 0.8$ (octagon) and $m = 0.9$ (plus). The solid line is the continuum zero mode with $\rho = 1.5$.
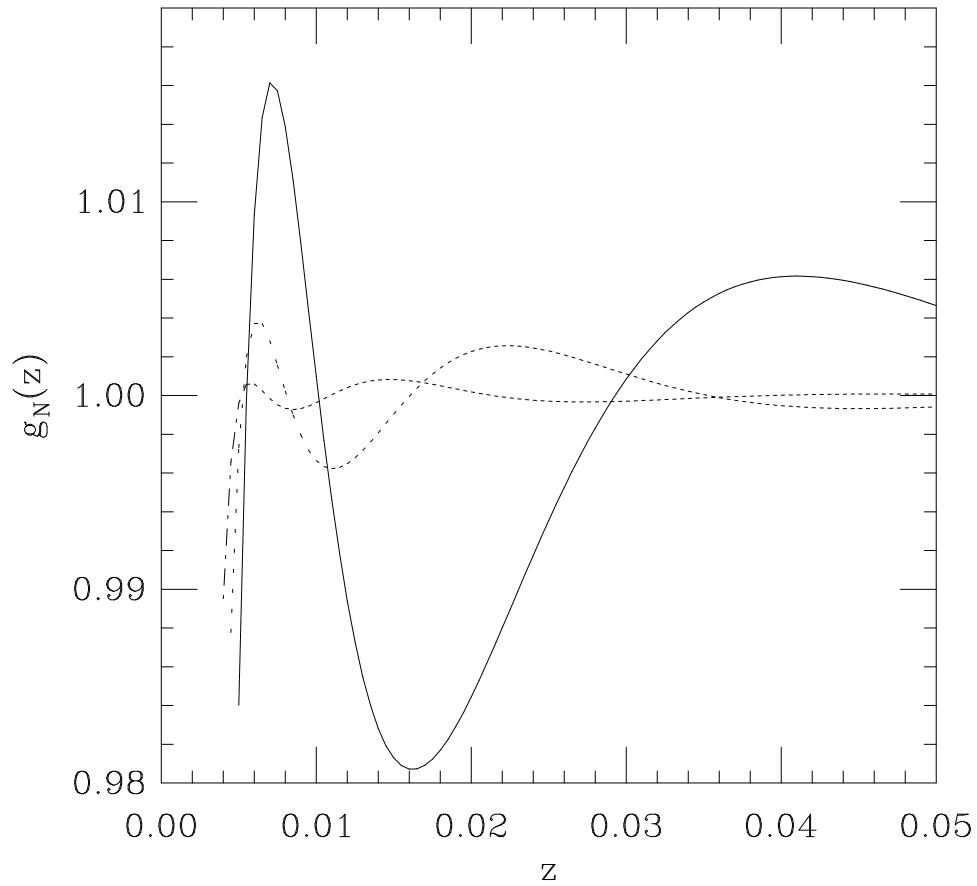
Fig. 3. The optimal rational function approximation $g_N(z)$ to $\epsilon(z)$ in the interval $[0.005, 1]$ for $N = 6, 8$ and 10. Shown is a detail of the region of largest deviation. Outside this region, the curves rapidly approach unity.
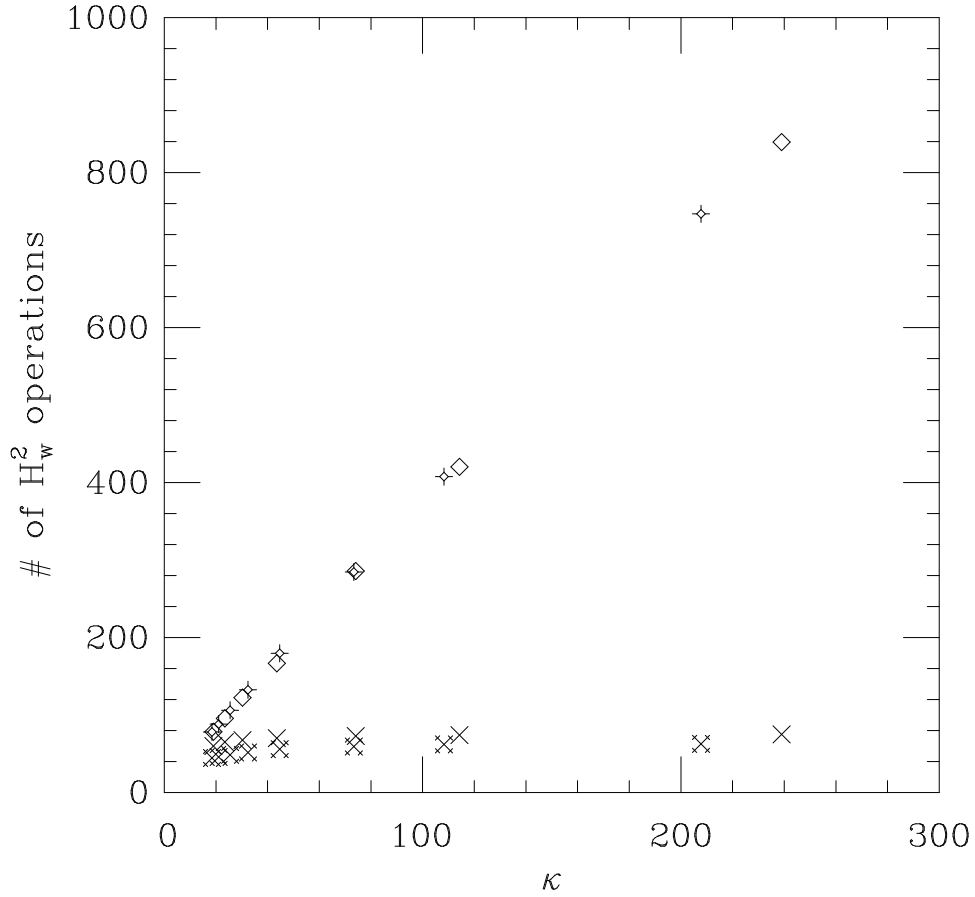
Fig. 4. Average number of $H_w^2$ operations for the optimal rational approximation and the fractional inverse methods to apply $\epsilon(H_w)$ on a vector versus the Wilson-Dirac operator condition number for the configuration in Fig. 1. The cross and fancy cross are for the optimal rational approximation below and above the crossing, resp. The diamond and fancy diamond are for the fractional inverse method below and above the crossing, resp.
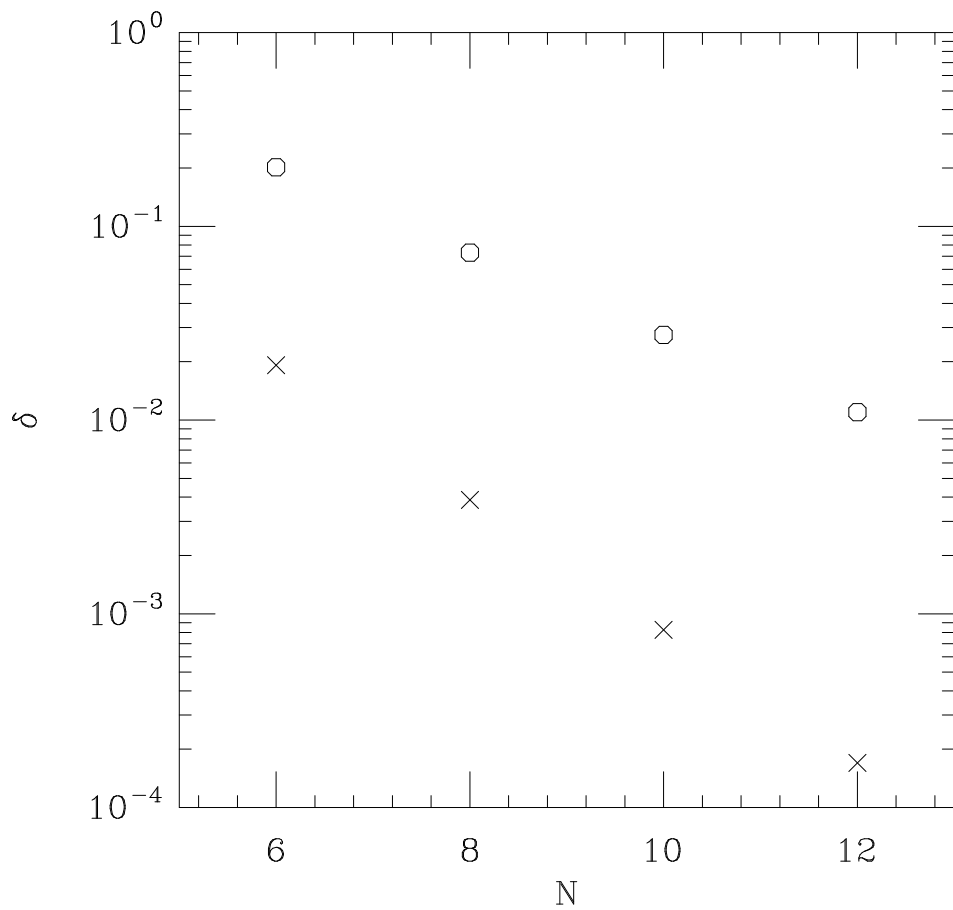
Fig. 5. The accuracy as a function of the number of poles for a fixed condition number. The crosses are for condition number $\kappa = 200$ and the octagons are for $\kappa = 1000$.
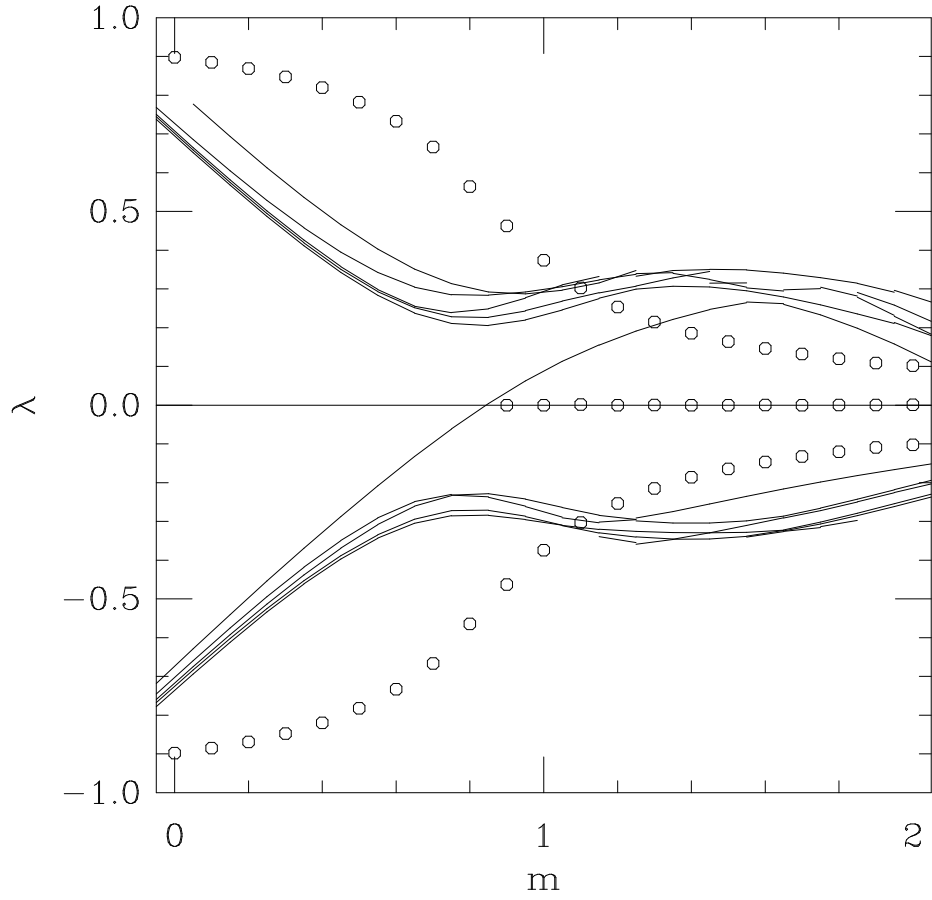
Fig. 6. The octagons describe the low lying spectrum of $H_o$ in a pure SU(2) gauge field background at $\beta = 2.5$. The zero mode found at $m > 0.8$ is singly degenerate and is associated with an instanton in the background gauge field. The lines are the spectral flow of $H_w$.
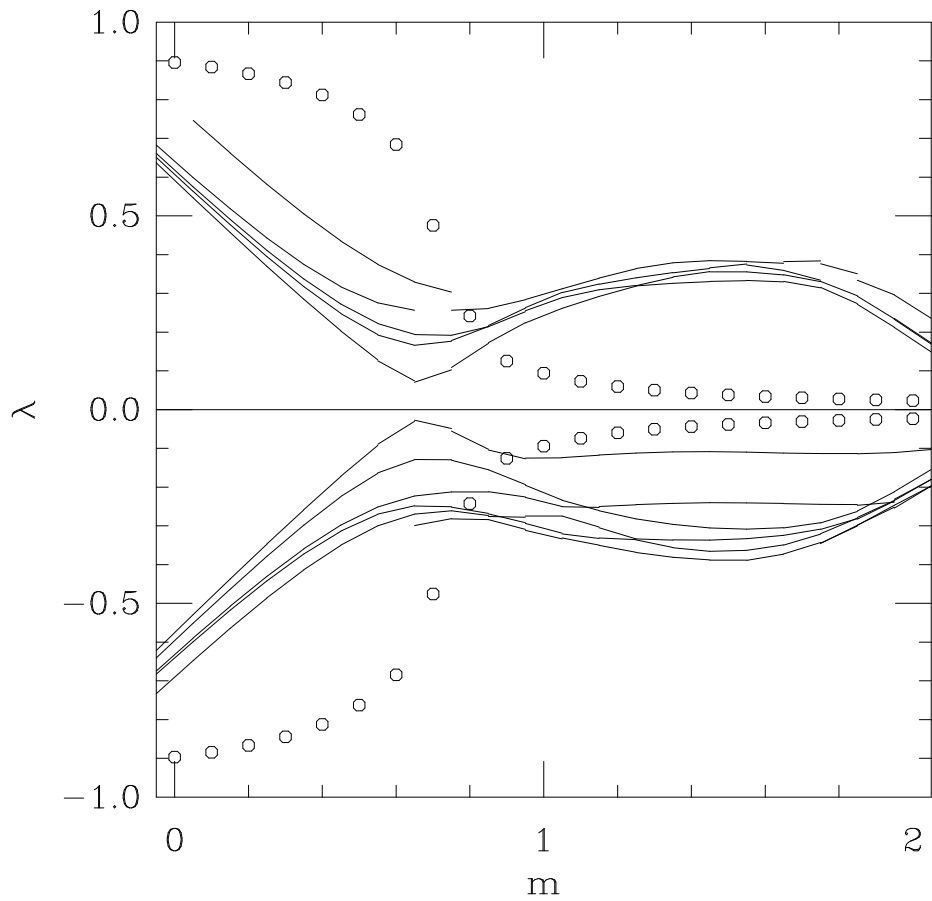
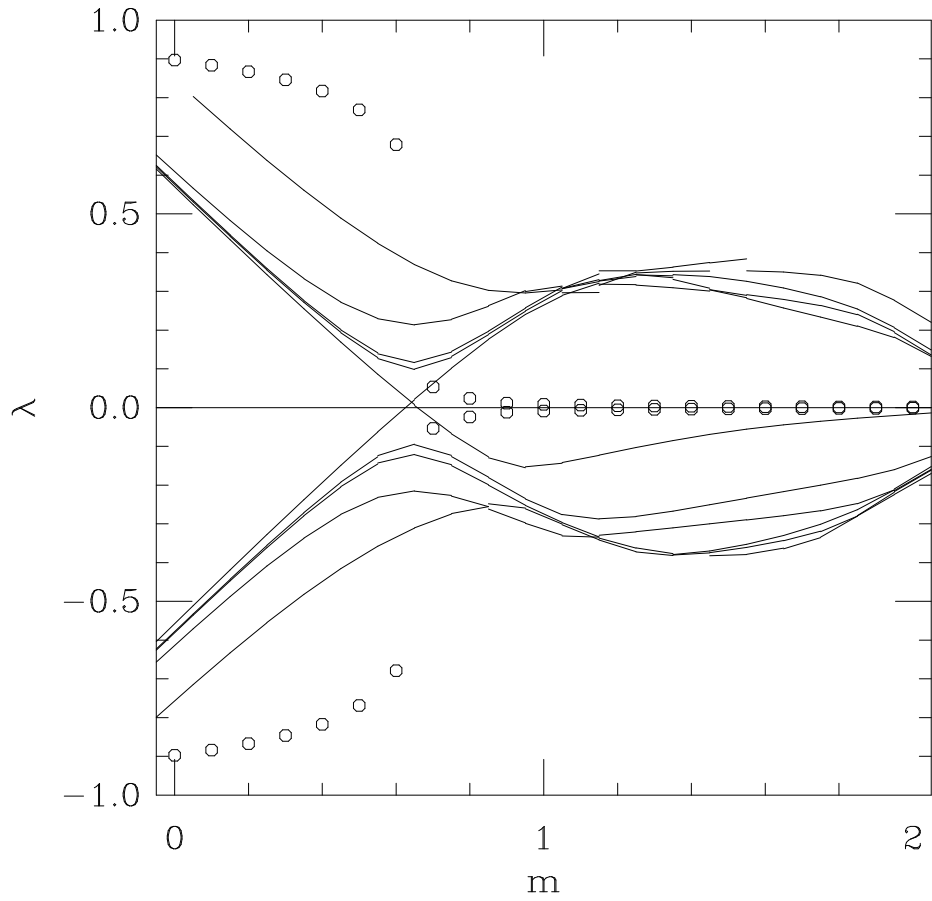Fig. 7. Same as in Fig. 6 for a different SU(2) configuration at $\beta = 2.5$.

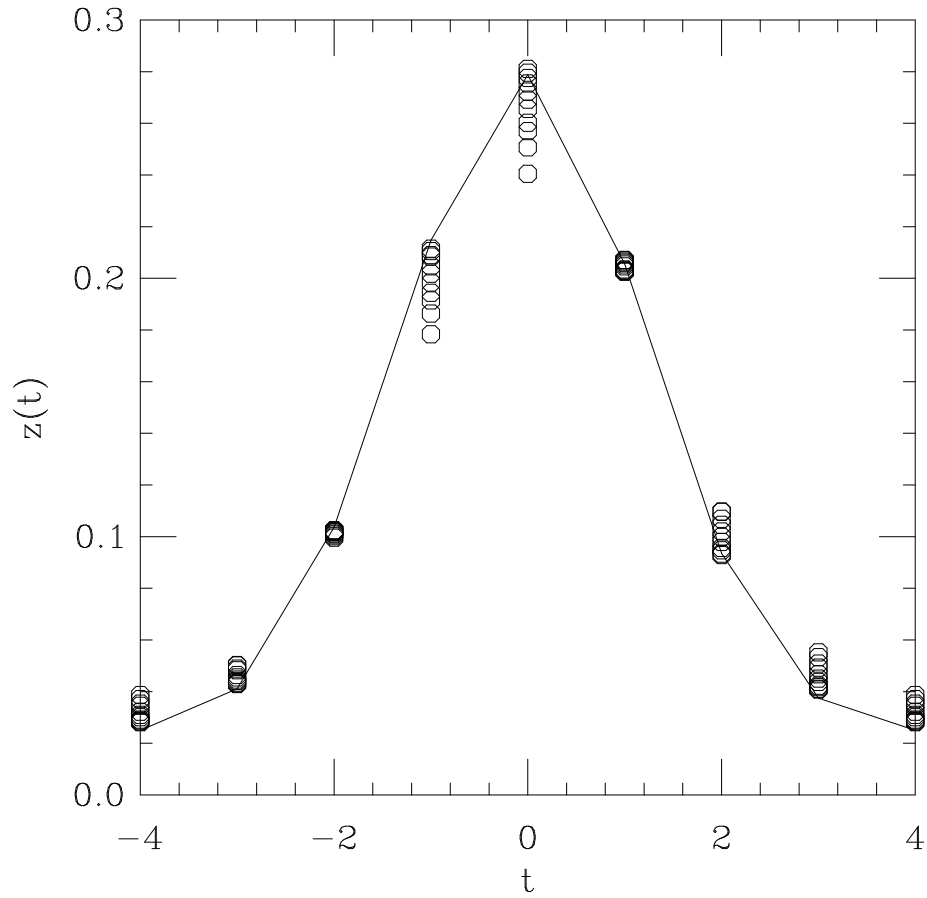Fig. 8. Same as in Fig. 6 for a different SU(2) configuration at $\beta = 2.5$.

Fig. 9. The mode associated with the zero eigenvalues in Fig. 6 for $m > 0.8$ is plotted with octagon symbols and compared with the zero mode of $H_w$ shown as straight line segments.